RESEARCH ARTICLE

High-efficiency silicon solar cells designed on experimentally achieved nano-engineered low-reflective silicon surface

S. M. Amir-Al Zumahi[1] · M. Khairul Basher[1,2] · Nourin Arobi[3] · M. Momtazur Rahman[2] · Ahmed M. Tawfeek[4] · M. A. Rafiq Akand[1] · M. Mahbubur Rahman[3,5] · M. Nur-E-Alam[2,5,6] · M. Khalid Hossain[1,7]

Abstract We explore the design and optimization of high-efficiency solar cells on low-reflective monocrystalline silicon surfaces using a personal computer one dimensional simulation software tool. The changes in the doping concentration of the *n*-type and *p*-type materials profoundly affects the generation and recombination process, thus affecting the conversion efficiency of silicon solar cells. To enhance solar cells' performance, copper nanoparticle (Cu-NP) assisted surface texturization has been employed on the silicon surface with resistivity 1–3 Ω.cm. The surface texturization assists in reducing the surface reflection of silicon by around 0.65%. The doping concentration and the layer thicknesses of a solar cell are optimized and found that 1×10^{14} cm^{-3} doping concentration at three different thicknesses (5, 10, and 15 μm) of the n-type region exhibit the maximum solar cell conversion efficiency of around 26.19%. The optimized design solution shows the best output parameters namely open-circuit voltage (V_{oc}) around 0.749 V, short circuit current (I_{sc}) about 3.987 A, and a fill factor of 26.19% that can be potentially useful for the fabrication of high-efficiency solar cells.

Keywords Monocrystalline · Silicon solar cell · Low surface reflection · Texturization · Doping concentration · PC1D simulation

Introduction

Since the first discovery of solar cells, energy photovoltaic power generation has been considered one of the most active and readily available renewable sources to achieve the green-sustainable global demand [1–3]. Over the last two decades, solar energy demand increased at an average rate of around 30% per annum [4]. Effective photovoltaic power generation depends not only on the number and types of solar cells but also on solar panel installation orientation (solar panel needs to be installed with a certain angle orientation depending on area or location). Silicon solar cells dominate the current photovoltaic market for several reasons, including materials availability, low bandgap, low cost, nontoxicity, long-term stability, and low absorption coefficient properties, among other types of solar cells like cadmium telluride solar cell (CdTe) [5], copper indium gallium selenide solar cells (CIGS) [6], gallium arsenide germanium solar cell (GaAs) [7], dye-sensitized solar cell (DSSC) [8, 9], etc. However, an enormous difference in efficiency between the laboratory and commercially available Si solar cells is always observed, which still opens the possibility for the researchers to conduct new research to acquire the possible highest efficiency

✉ M. Nur-E-Alam
m.nur-e-alam@ecu.edu.au

✉ M. Khalid Hossain
khalid.baec@gmail.com; khalid@kyudai.jp

1 Atomic Energy Research Establishment, Bangladesh Atomic Energy Commission, Dhaka 1349, Bangladesh

2 School of Science, Edith Cowan University, 270 Joondalup Drive, Joondalup, WA 6027, Australia

3 Department of Physics, Jahangirnagar University, Savar, Dhaka 1342, Bangladesh

4 Department of Chemistry, College of Science, King Saud University, 11451 Riyadh, Saudi Arabia

5 Institute of Sustainable Energy, Universiti Tenaga Nasional, 43000 Kajang, Selangor, Malaysia

6 School of Engineering and Technology, Central Queensland University Australia, Melbourne, VIC 3000, Australia

7 Department of Advanced Energy Engineering Science, Interdisciplinary Graduate School of Engineering Sciences, Kyushu University, Fukuoka 816-8580, Japan

in commercial solar cells [10–12]. Many researchers worldwide are working on more intensive studies on silicon solar cells, mainly improving solar cells' efficiency and setting up their easy, eco-friendly, and more cost-effective commercial productions till today [13, 14].

A substantial number of studies have been carried out to improve silicon solar cells' efficiency and overcome other relevant bindings related to the cell's stability, reliability, and light-trapping properties. However, most of them are reported to improve Si cells' efficiency by tailoring further structural and surface modifications. Most of the best-reported results are found simulation-based, whilst any part of their practical demonstration is yet to be developed according to the scholars' statements [15–22]. However, the fabrication of crystalline Si cells with modifying and new concepts has recently become a pioneer research area for improving practically highly efficient silicon cells [23, 24]. Gim Chen et al. [15] and their research group demonstrated that an optimized IPA-free alkaline (KOH) texturing is viable for large-scale manufacturing in heterojunction Si solar cells in the existing KOH/IPA. Additionally, the benefits of utilizing a non-IPA additive instead of IPA were also noticed, which increased the consistency of the texture morphologies for improving the efficiency of Si solar cells as investigated by S. C. Baker-Finch et al. [16]. Min Su Kim et al. [17] have reviewed the principle and application of surface texturization methods utilizing micro/nanoscale structures on the surfaces of solar cells. The surface modification processes utilizing microscale and nanoscale structures with unique anti-reflective or light-trapping optical properties leads to enhance the efficiency of solar cells. Other studies also proposed various optimizing parameters such as new etchant [19–21], two-step texturing by controlling temperature [20, 25], anti-reflecting coatings [26], front and back contact structure [27, 28] for the reduction of incident light loss to increase the efficiency of the solar cells. Whilst for an industrial mass production of high-efficiency silicon solar cells, several design or technology limitations, related to surface passivation, metal contacts, material quality, and cell structures require further improvement [18].

Several approaches have been named and published by scientists and researchers to enhance the light-absorbing ability of silicon solar cells by reducing light reflection from the solar cells' front surface and raising the path length of light within the substrates. Surface modification is one of the well-known hypotheses to reduce the front surface reflection losses. Surface texturization and nano-structured gratings developments are usually used to improve the light gain characteristics of the solar cells' base structures [27–34]. However, the manufacturing cost of the surface texturization method is widely used (through different physical and chemical etching methods) to improve solar cells' performance by reducing the silicon surface's reflection coefficients. A
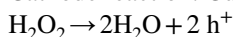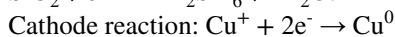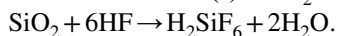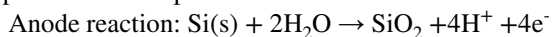
significantly low reflection coefficient (0.652%) has been achieved by our group, and no reports are available in the literature to attain a practical surface with a reflection value of less than one [35]. We used a low reflectance value of the textured surface in PC1D as the reflection parameter to gain the maximum efficiency for Si solar cells using different doping concentrations of three doping regions (low, medium, and high) for the n-type layer.

In this work, we model and optimize silicon solar cells' parameters on experimentally achieved nano-engineered low-reflective silicon surfaces and investigate the possible modeled outputs in terms of electrical properties with different doping concentrations. We analyze the efficient engineering and development of monocrystalline silicon cells utilizing state-of-the-art tools (PC1D software) to modify the carrier concentration of n-type and thickness of both layers (n-type and p-type). We briefly describe the glimpse of copper (Cu) nanoparticle-assisted silicon surface modification and the best obtained optical and structural properties of a texturized silicon surface. Using PC1D software, the influences of doping concentration-dependent minority carrier diffusion length, generation-recombination, series resistance, and shunt resistance nano-engineering on open-circuit voltage, current density, fill factor, and overall efficiency are studied in three different regions. Experimentally, it is very tough to find out the specific doping regions for highly efficient Si solar cells. That is why we mention three different regions by PC1D simulation to specify the best one for experimental purposes. More preciously, three doping regions (low, medium, and high) are investigated to realize higher efficiency in tailoring different doping concentrations for the n-type layer. The layer modification of very low reflectance n-type frames indicates that the conversion efficiency can be achieved from monocrystalline silicon solar cells in a low-level doping zone as high as 26.19%. The simulation results show how to identify the ideal region for doping concentration to achieve time-consuming, low-cost, and sustainable solar cells when going through the experimental procedure. Finally, the overall objectives of this work are: (i) Design and optimization of high-efficiency solar cells on experimentally achieved nano-engineered low-reflective silicon surfaces using PC1D simulation software tool; (ii) Investigation of doping (n-type and p-type materials) concentration effects variations on the generation and recombination process and the conversion efficiency of silicon solar cells; (iii) Optimize the doping concentration and layer thicknesses of the solar cell to achieve maximum conversion efficiency, with 1×10^{14} cm^{-3} doping concentration at three different thicknesses (5, 10, and 15 μm) of the n-type region exhibiting the highest efficiency of around 26.19%; (iv) Determine the best output parameters, including open-circuit voltage (Voc) around 0.749 V, short circuit current (I_{sc}) about 3.987 A, and a fill factor (FF) of 26.19%

for the fabrication of high-efficiency solar cells; (v) Study the influences of doping concentration-dependent minority carrier diffusion length, generation-recombination, series resistance, and shunt resistance nano-engineering on the electrical properties of the solar cells; and (vi) Investigate the impact of surface passivation, metal contacts, material quality, and cell structures on the industrial mass production of high-efficiency silicon solar cells.

Modeling and simulation

A manual sheet metal cutting machine was used to manually cut flat zinc plates (99% pure, collected from the local market), 2 mm thick, into 2 cm × 2 cm. A bench polisher grinder machine was then used to polish the samples. A flap wheel with 80-grit was used to remove the corrosion and imperfections. After that, Zn plates were polished using 120-grit flap wheels to achieve the necessary mirror finish. The polished Zn plates were cleaned with acetone in an ultrasonic bath for 10 min, then with ultra-pure deionized (DI) water for 10 min to remove any lingering dust or residue from the mirror-polished surface. To observe the impact of etching on ZnO development, certain samples were then chemically etched using 5% HCl in ethanol for a maximum of 3 min. However, multiple trials and mistakes have been carried out using a minimum volume (1%) concentration of HCL to up to 10 vol% added to ethanol by keeping the etching duration fixed to determine the best chemical compound solution (HCL in ethanol) and the optimal etching process time. Once we found the best solution, we varied the etching time from 1 to 5 min to find the best etching time duration. The reaction that happened during the etching process can be explained in a simple chemical formula.

Anode reaction: $Si(s) + 2H_2O \rightarrow SiO_2 + 4H^+ + 4e^-$

$SiO_2 + 6HF \rightarrow H_2SiF_6 + 2H_2O.$

Cathode reaction: $Cu^+ + 2e^- \rightarrow Cu^0$

$H_2O_2 \rightarrow 2H_2O + 2h^+$

The solar cell efficiency enhancement depends on the light trapping and profound distribution of light from the surface to the conduction face. The roughness of the surface and reflection of the modified wafer through surface texturization help minimize the top surface reflection and thus improve the light trapping and scattering properties.

Cu nanoparticles assisted silicon surfaces texturization and characterization

Surface texturization is one of the most promising and has become a standard process for preparing cost-effective and low-reflective rough surfaces. In this work, boron-incorporated Si wafers (of the monocrystalline shelves) were used to prepare texture and low reflective substrates by applying the Cu nanoparticle-assisted chemical surface texturization process. Before the final chemical texturization process, p-type monocrystalline silicon wafers < 100 > (size about 12.5 × 12.5 cm^2) of thickness around 200 μm, and resistivity of 1–3 Ω.cm were processed for metal-assisted chemical etching through a required rigorous chemical cleaning process as detailed in Ref. [35]. During the metal-supported chemical engraving treatment, the Cu- nanoparticle adhesion was tested by dispensing $Cu(NO_3)_2.3H_2O$:HF:H_2O_2:DI aqueous liquefaction for different process times at different temperatures. In this chemical process, the Cu-NPs usually get compacted within the silicon wafer by notching a pyramid-like inverted appearance features, as demonstrated in Fig. 1. Figure 1 shows a schematic diagram of the process flow of surface engineering, and characterization applied to achieve the best (lowest reflective and inverted pyramid-shaped) texturized silicon surface. The irregular surface damages of raw wafers showed a random distribution of inverted pyramid-shaped features on Si substrates. However, the effect of temperature and process time duration were evaluated from experimentally obtained optical and structural properties of chemically etched monocrystalline silicon surfaces.

Best-obtained properties of nano-engineered silicon surfaces

The light-trapping function can be understood from the measured reflectivity properties of different textured wafers. Figure 2 represents a schematic diagram of a monocrystalline silicon solar cell device and the measured best obtained optical (surface reflectance) and the morphological properties of chemically modified (optimally treated) silicon wafers. The surface reflectance was measured for a range of spectral regions by using ultraviolet–visible spectrophotometry (Perkin Elmer Lambda1050, USA). The surface morphology was investigated using the AFM and field emission scanning electron microscopy (FESEM, JSM-7600F, USA) as well as an elemental composition by EDX analysis (Oxford instruments microanalysis group 6699 ATW). An optimized electrochemical etching recipe was determined from the time and temperature-dependent Cu-assisted textured surface properties. It was observed that the average reflectance value was observed to differ from 0.6–6.15% based on the process time and temperature, which was smaller than that of the main substant. It was also observed that the process temperatures greatly influenced the optical reflection and the surface texturing properties more than the process time duration. High temperatures mainly accelerated the oxidation process on the silicon surface. However, the increasing temperature helped the formation of nano-pits, which did not significantly impact the light-absorbance properties of etched Si surfaces. It was observed that Cu-assisted chemical etching performed at 50 °C for
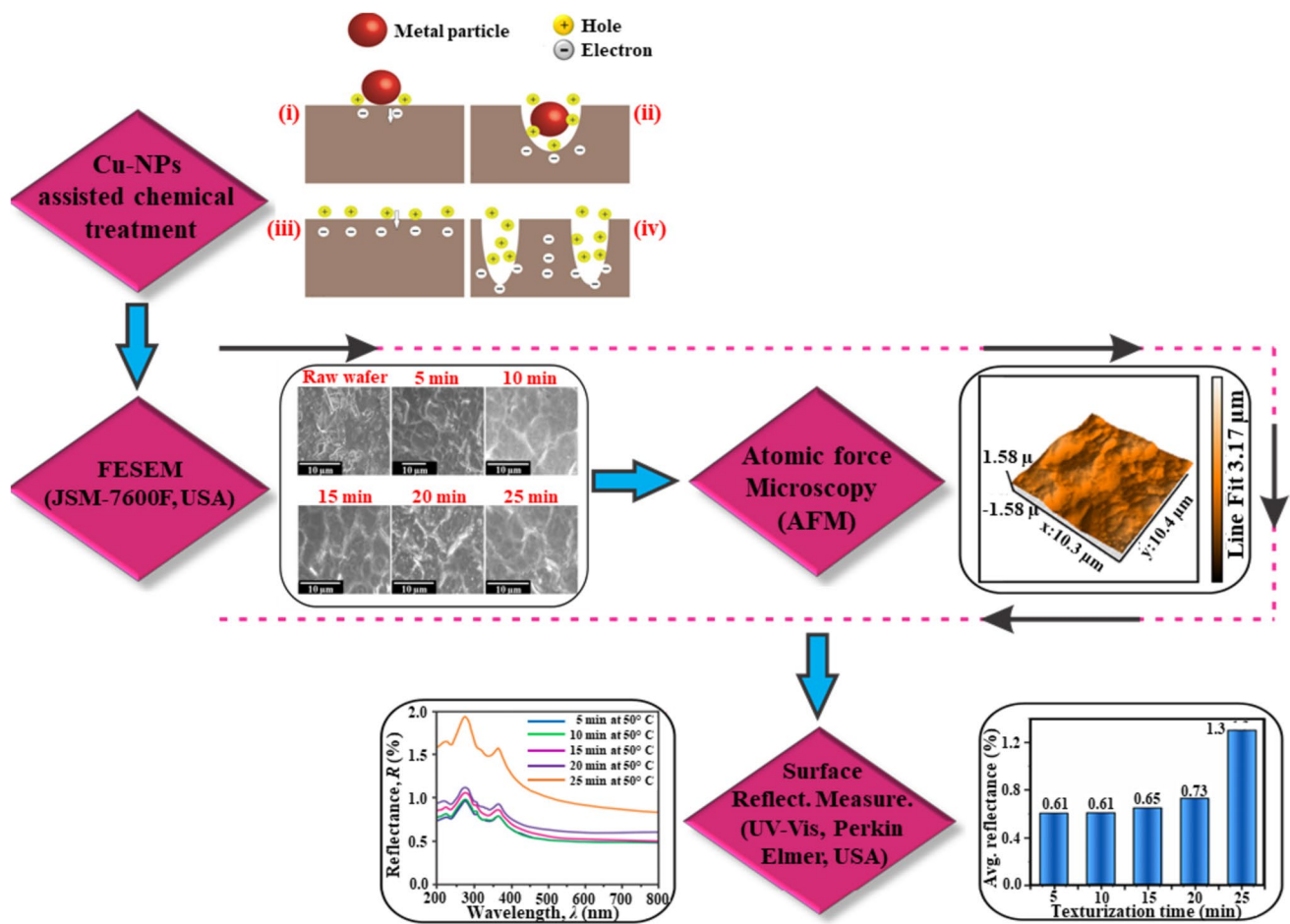
Fig. 1 Process flow of silicon surface texturization and characterization to obtain the low refractive Si surfaces. The top section explains the possible electrochemical process (i–iv) that took place between Si and Cu + ions through Cu-NPs-assisted anisotropic etching mechanism (basically the result of an electrochemical energy difference between Cu + /Cu-NPs and Si). The middle and bottom sections represent a glimpse of the obtained structural and optical results of the entire chemical process [35]

15 min showed the lowest reflection about 0.65% (averaged) simultaneously with the presence of a large area of irregular inverted pyramidal nanofeatures having an average depth of around 1.58 μm. The best obtained optical and structural properties on silicon wafers are helpful in designing and fabricating next-generation, highly efficient, cost-effective, and commercial silicon solar cells.

Design consideration and optimization of Si solar cells

Simulation tools always play essential roles in providing proficient information helpful to experimental work to develop new and existing but modified and improved solar cells. Well-defined simulation software helps the understanding and the changes of system parameters, faster configuration, low-cost operation, time, and risk reduction [36]. In this work, a typical silicon solar cell model has been chosen for simulation using a very simple and commercially available PC1D (Version 5.9) simulation software package. PC1D is

a one-dimensional simulator widely employed in solar cell research related to solar cell design, engineering, optimization, and calibration. This well-developed program offers a fast and easy user interface with state-of-the-art flexibility, and a wide variety of input parameters and output options are available to perform device simulation with higher accuracy [36–38]. Various types of thin film solar cells have been successfully designed, modeled, and optimized for cell parameters to obtain the highest efficiency in the solar cells toward developing cost-effective commercial solar modules [39–43]. Figure 2a represents a schematic diagram of a monocrystalline silicon solar cell device. Different parameters of a flexible internal model, including series resistance, shunt conductance, and shallow diffused emitter, are presented within the diagram. The thickness of the *p*-type doped region of the photovoltaics is comparatively thicker (about 194 μm) compared to that of the *n*-type region (Fig. 2a). The *n*-type doping area's thickness is around 6 μm, as can be found in the top texturized inverted pyramidal-shaped
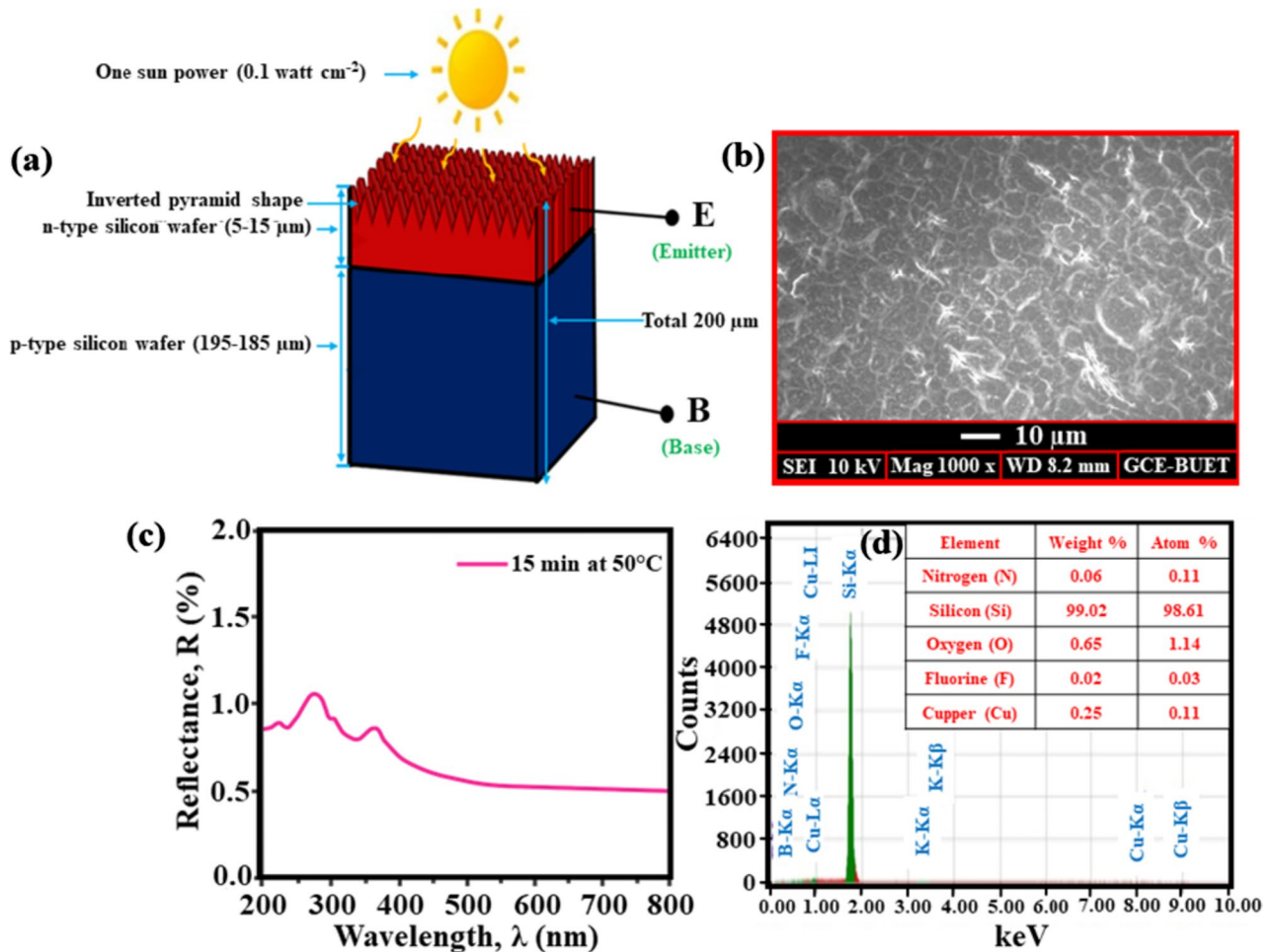
Fig. 2 **a** The schematic diagram of a PC1D silicon solar cell model, **b** SEM image of obtained surface morphology of textured wafer, **c** optical reflectance versus wavelength graph of the inverted pyra-mid arrays obtained via Cu-assisted etching performed at 50 °C for 15 min, and **d** shows the EDX analysis of the texturized surface of the substrates. Reproduced with permission from Ref. [35]

area. The surface area of the modeled solar cell was kept at around 10×10 cm^2, and the model simulation performances were controlled with the maximum input power of one sun (0.1W cm^{-2}). We used the best obtained low surface reflection of around 0.652% in our experiment for the value of external front reflection.

The numerical simulation software PC1D (developed by the University of New South Wales, Australia) contains library files with the crystalline semiconductors' parameters and files of the solar spectrum (AM0 and AM1.5) photovoltaic technology for the development of solar cells and their optimization. SCAPS-1D simulation software relies on two fundamental semiconductor equations for its basic operation. One of them is the continuity equation, which describes the behavior of electrons and holes in steady-state conditions, and the other is the Poisson equation, which is applied to free electrons and holes in the conduction and valence bands [44, 45]. The main window of PC1D contains five essential parts: a device, Region-1,

Excitation, Results, and Device schematic. Simulation optimization was performed by connecting the excitation mode by changing the number of times and fixing the base circuit maintaining all the resistances to 0 ohms. The part 'excitement' of this software simulates the solar cells' behavior considering irradiation conditions, operating temperature, and other parameters. The part 'results' offers to enable the standards of open-circuit voltage (V_{oc}), close circuit current (I_{cc}), and the maximum power (P_{max}) leading to obtaining the current–voltage curves for the simulated cells under the standard excitation power for AM1.5 solar illuminations. The parameters shown in the simulation optimization are mentioned in Table 1.

All the parameters were adjusted according to the simulation tools required to increase or decrease the doping impact and properties. However, the irregular inverted shapes were neglected for the simplicity of software purposes (consider surface reflection value only) and to understand the parameter variations impact in this experiment.

Table 1 Values of the parameters used in the PC1D solar cell simulation

Parameter	Value
Surface area	10×10 cm^2
Bandgap	1.124 eV
Dielectric constant	11.9
Thickness	n-type (5–15 μm)
	p-type (195–185 μm)
Exterior front reflectance	0.652%
Refractive index	3.58
Intrinsic concentration at 300 K	1×10^{10} cm^{-3}
Bulk recombination (τn and τp)	1000 μs
Excitation mode	Transient, 16-time steps
Base circuit	Sweep from -0.8–0.8 V
Temperature	25 ℃
Spectrum	AM 1.5
Constant intensity	0.1 W cm^{-2}

Table 2 The range of doping levels used in monocrystalline silicon wafer preparation

Doping	Dopant concentration (cm^{-3})	Simulated dopant concentration (cm^{-3})
Low	Less than or equal to 10^{14}	1×10^{14}
Moderate	10^{14} to less than 10^{18}	1×10^{17}
High	10^{18} to less than 10^{20}	1×10^{19}

Results and discussions

The simple mechanism of how photovoltaic cell generates electricity by absorbing solar radiation is the excitation of electrons in the valence band and their mobility toward the next band (conduction). Photons of higher energy than the bandgap of a semiconductor excite and transform the conduction band and forsake extensive equal counts of holes in the valence band. As a result, when the charge carriers of electrons and holes shift in the reverse way of the device, a net electric current occurs. However, the electrical conductivity in semiconductors figures on the carrier's concentrations (electrons/holes). The doping concentration helps to manipulate the concentration levels of electrons, and holes on the silicon wafer, thus influencing internal properties [37, 46]. The doping action can be understood with the aid of the bonding model and the atomic structure of semiconductors. Table 2 shows the range of doping concentration that was used to simulate the monocrystalline silicon cells in this research work [37]. The incorporating concentration and the emitter layer's depth were chosen to absorb the most incoming incident sunlight spectrum.

The incorporation concentration of the emitter affects the overall device performance significantly.

For solar cell, design and simulation, a fixed concentration of p-type silicon wafer (1×10^{14} cm^{-3}, moderate doping) was considered while the n-type silicon wafer concentration was varied. The surface doping effect for the p-type and n-type silicon wafers can be described by **Eq.** 1 [47]:

$$S(N) = S_0 \left(\frac{N}{N_{\text{onset}}}\right)^{\alpha}, N > N_{\text{onset}} \tag{1}$$

where, $S(N)$, $S0$, N, Nonset, and α are surface recombination velocity, absolute surface recombination velocity, normal surface concentration, doping concentration for onset, and absorption coefficient, respectively. From the above expression, the nature and properties of the surface treatment process can be very effectively characterized.

Effect of doping profile on generation and recombination

When the solar cells' surface absorbs solar radiation (steady-state illumination condition) spectrum, photogeneration occurs. The electric charges may travel as an electric current to an external circuit or recombine within the system. The cumulative photogeneration and recombination from the front exterior, as just a function of the Si distance, can be considered in a concise overview in Fig. 4 with three different levels of doping concentrations and three different p-type and n-type thicknesses. For a low level and a moderate level of doping concentration (as shown in Fig. 3), the cumulative photo generation increases rapidly for a specific time; afterward, it grows slowly and becomes constant. On the other hand, the recombination shows a straight line toward the center, which confirms the generation of a moderate number of carriers with a high recombine rate. For the high level of doping concentration, irregular shapes of response were observed in the graph (inset Fig. 3a-c with blue line spectrum, first increasing straightly and later becoming nearly constant horizontally). All the generation curve shows isotropic properties with a very comparable value whereas recombination shows anisotropic. 1×10^{14} cm^{-3} n-type doping concentration shows an intermediate position between 1×10^{17} cm^{-3} and 1×10^{19} cm^{-3} for all the graphs in Fig. 3 owing to the higher extinction coefficient [48]. The recombination (virtually the reverse process of generation) for silicon material is affected by temperature, doping, and electric field, which are experimentally proved by previous literature [49–52]. The anisotropic recombination process may occur due to the doping concentration.
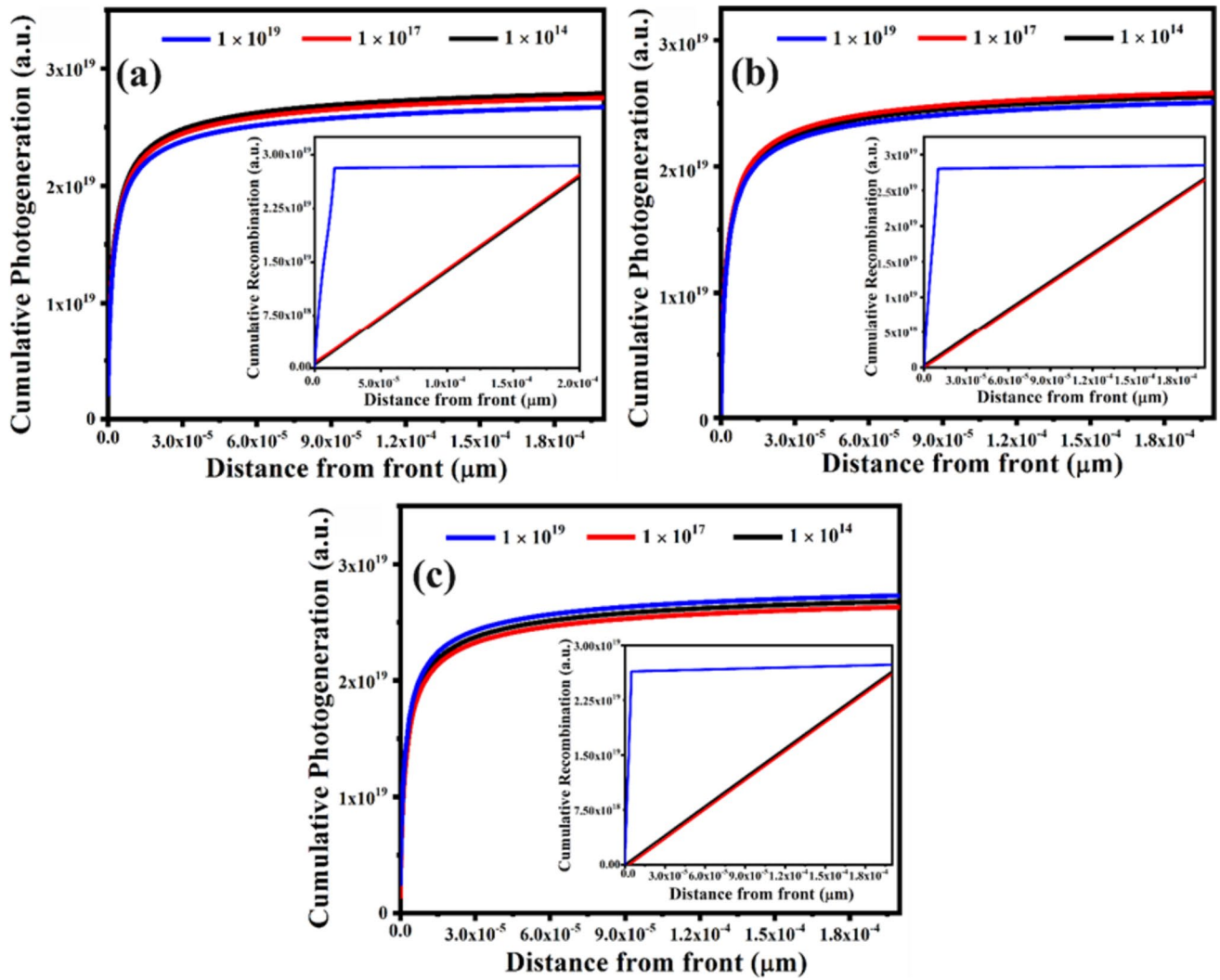
Fig. 3 Cumulative generation and recombination graph for **a** p185, n15 nm **b** p190, n10 nm, and **c** p195, n5 nm with different levels of doping concentration (1×10^{14}, 1×10^{17}, and 1×10^{19} cm^{-3})

Effect of doping profile on output parameters

The current–voltage characteristic curve is one of the most common methods or graphical representations of determining the monocrystalline silicon solar cell function among the current flowing and the voltage applied throughout the system. The current versus voltage graph of a different cell with different thicknesses (*n*-type and *p*-type) and doping concentration (*n*-type) for comparing their conversion efficiency are exhibited in Fig. 4 and summarized in Table 3. Different concentration such as 1×10^{14}, 1×10^{17}, and 1×10^{19} cm^{-3} was used to calculate the efficiency for three different thickness i.e., *p*195, *n*5 μm; *p*190, *n*10 μm; and *p*185, *n*15 μm. As can be seen from the *I-V* curves estimated under one sun illumination, the I_{sc} and V_{oc} are the same for 1×10^{14} cm^{-3} and 1×10^{17} cm^{-3} doping concentration and decreases for

1×10^{19} cm^{-3} doping for three different thickness of monocrystalline cells (Table 3).

The tangent slopes (*m*1 or 2) of the I-V plots across V_{oc} and I_{sc} give 1/series resistance (1/R_s) and 1/shunt resistance (1/R_{sh}) respectively, and the opposite of such tangent slopes (*m*1 or 2) expresses the series and shunt resistance explicitly (**Eqs.** 2 & 3) [53]:

$$R_{sh} = -\left.\frac{dV}{dI}\right|_{V=0} = -\frac{1}{m_1} \tag{2}$$

$$R_s = -\left.\frac{dV}{dI}\right|_{I=0} = -\frac{1}{m_2} \tag{3}$$

The gradient of the *I-V* graph for the solar cell was calculated using d*I* and d*V* from the above equation, given R_{sh} and R_s values.
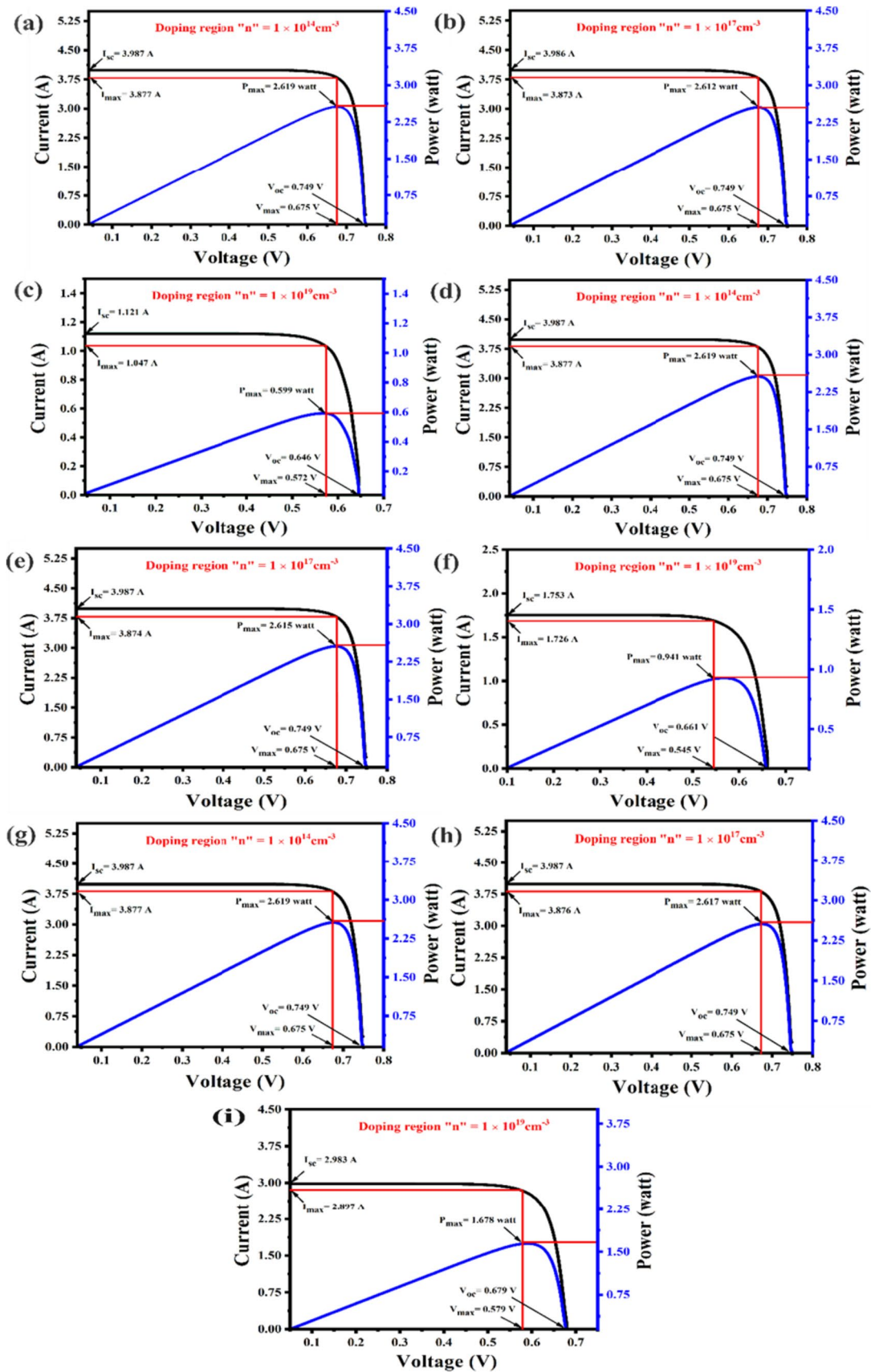
Figure 5 demonstrates how the shunt and series resistances for different devices can be decided from an inverse slope. The calculated values for shunt resistance and series resistance are outlined in Table 3 for different concentrations and solar cells. Figure 6 shows the contrast of shunt resistance and series resistance for three other solar cells with varying three different concentrations of the n-type region. In this case, the photovoltaic parameter such as shunt resistance decreases following increasing the p-type thickness and reducing the n-type thickness. In contrast, series resistance shows the opposite behavior and decreases efficiency from 26.19 to 5.99%, similar to the published report [54]. Marko Turek et al. introduced that the most crucial factor in gaining a cell's performance is to enhance the shunt resistance as much as possible and keep the series resistance level as low as feasible [55]. This view fully supports the results of the shunt resistance and series resistance we tabulated in Table 3.

The series resistance of the solar device for several concentrations maintains an increasing straight-line pattern. Where 1×10^{14} cm^{-3} and 1×10^{17} cm^{-3} doping concentration spectacles have the same value (Table 3 and inset Fig. 6), but a high-level incorporating concentration of 1×10^{19} cm^{-3} for all the photovoltaics exhibits high resistance. The average distance between the generation points and the initial of the recombination process is diffusion length dependent on solar cell performance [56]. Therefore, diffusion length is a vital parameter for solar cell efficiency variation. The impact of dopant density on diffusion length to tailoring the different thicknesses of *p*-type and *n*-type layers for efficiency variation is illustrated in Fig. 7. The diffusion lengths have progressively grown up to 0.002 μm for all lengths of 1×10^{14} cm^{-3} and 1×10^{17} cm^{-3} doping concentration for different thicknesses, whereas above 0.006 μm for 1×10^{19} cm^{-3}. Afterward, with the rise in distance from the front, a constant value of diffusion length was achieved. For *p*195, *n*5 μm; *p*190, *n*10 μm; and *p*185, *n*15 μm silicon solar cells, the widths of the emitter regions in this measurement are 5×10^{-6} μm, 1.01×10^{-5} μm, and 1.50×10^{-5} μm respectively.

Diffusion length in the emitter part for all thicknesses is much shorter (from 0 to 0.0015 μm, as shown in Fig. 7). Because of the emitter's high dopant density, the diffusion length limit (emitter region) decreases as reported in the Ref [57]. Here, the emitter's thickness is less than that of the diffusion length, resulting in a significantly high probability of charge collection [58]. Usually, for higher recombination, the emitter region requires having two or more times doping than the base region. Therefore, higher recombination mostly adheres to the disproportionate relationship with diffusion length [59] which supports our previous recombination graph (Fig. 4), is evidence.

Figure 8a shows that a significant improvement in cell performance can be observed when doping concentration rises from 1×10^{14} cm^{-3} to 1×10^{19} cm^{-3}. The concentration of *n*-type silicon wafer considerably affects the fill factor (FF) of the cell, decreasing rapidly when the concentration is 1×10^{19} cm^{-3}. This graph maintains the same pattern as the previous literature of Haris Mehmood et al. [60] Fig. 8b demonstrates the seesaw of efficiency with doping concentration (*n*-type) under three different thicknesses. As the solar cell's doping concentration enhances from 1×10^{14}–1×10^{19} cm^{-3}, the efficiency also decreases and becomes very similar to all cells except 1×10^{19} cm^{-3} concentration. A maximum efficiency value of 26.19% is achieved for three separate solar cells with a doping concentration of 1×10^{14} cm^{-3}. The explanation is that the doping (for *n*-type) decrease will enhance photo-generated carriers' selection and increase conversion output [61]. We can see that as the n-type thickness increases and the *p*-type thickness decreases, cell performance decreases exponentially. Therefore, the thickness of these three separate solar cells influences pairs of electron holes [62, 63]. Finally, the result shows that the efficiency for *n*-type doping concentration (1×10^{14}–1×10^{19} cm^{-3}) with a textured wafer by exterior front reflectance (0.652%) varied from 26.19–5.99%.

In summary, we affirm that a low level of *n*-type doping concentration shows an intermediate position between moderate and high levels with a high extinction coefficient as in the following literature [48]. Thereby generation and recombination for lower levels show higher and lower values respectively under abridged diffusion length than other doping concentration levels. Moreover, shunt resistance is higher, and series resistance is lower for low-level doping concentration, indicating higher efficiency than other levels [55]. Recently, Galib Hashmi et al. introduced a 20.35% efficient simulated monocrystalline Si solar cell by PC1D with different doping concentration regions of pyramid surface architecture [37]. Nevertheless, in this study, the optimized parameters, including less reflection, inverted pyramid structure, and several doping concentrations help us achieve a maximum efficiency of 26.19% for the lower level at 1×10^{14} cm.$^{-3}$. Finally, low-level doping concentration indicates a rising pattern from photon to electrical conversation than other two-level doping concentrations. Furthermore, our simulated results are very much comparable with the latest achieved efficiency (26.8 ± 0.4) in the crystalline silicon solar cell and other silicon solar cells [64].

Table 3 Data of doping concentrations and photovoltaic parameters of monocrystalline silicon solar cell

Thickness of the layer (µm)		Doping concentration (cm^{-3})		I_{sc} (A)	V_{oc} (Volt)	P_{max} (Watt)	Shunt resistance (kΩ)	Series resistance (Ω)	Fill factor (%)	Efficiency, η (%)
n-type	p-type	n-type	p-type							
5	195	1×10^{14}	1×10^{14}	3.987	0.749	2.619	10	0.0085	87.70	26.19
		1×10^{17}		3.987	0.749	2.617	8.3	0.0085	87.63	26.17
		1×10^{19}		2.983	0.679	1.678	5.3	0.015	82.85	16.78
10	190	1×10^{14}		3.987	0.749	2.619	2.33	0.0077	87.70	26.19
		1×10^{17}		3.987	0.749	2.615	2.08	0.0077	87.57	26.15
		1×10^{19}		1.753	0.661	0.941	1.01	0.028	81.21	9.41
15	185	1×10^{14}		3.987	0.749	2.619	2	0.0063	87.70	26.19
		1×10^{17}		3.986	0.749	2.612	1.9	0.0063	87.49	26.12
		1×10^{19}		1.121	0.646	0.599	1.5	0.034	82.72	5.99
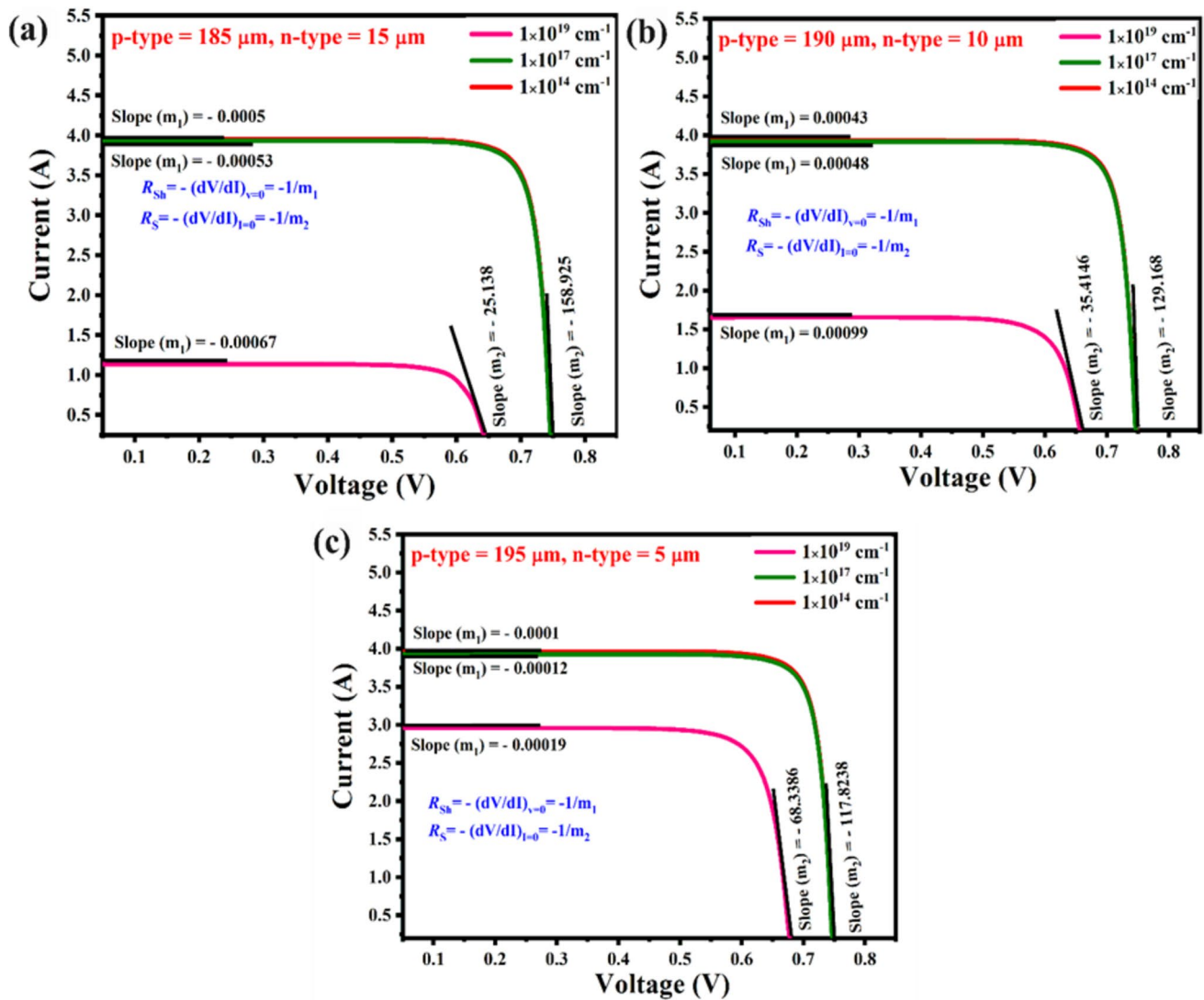
Fig. 5 Series resistance and shunt resistance calculation using the slope of I–V characteristic curves for three different configurations **a** p185, n15 µm **b** p190, n10 µm, and **c** p195, n5 µm
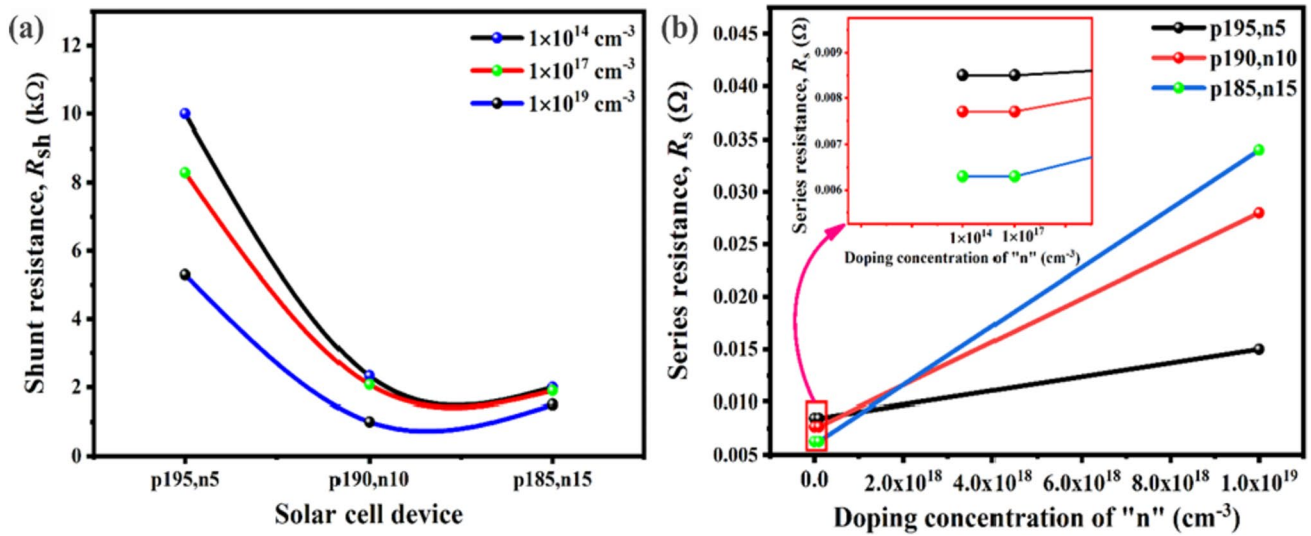
Fig. 6 Comparison of **a** shunt resistance and **b** series resistance for three different configurations *p*185, *n*15 μm; *p*190, *n*10 μm, and *p*195, *n*5 μm
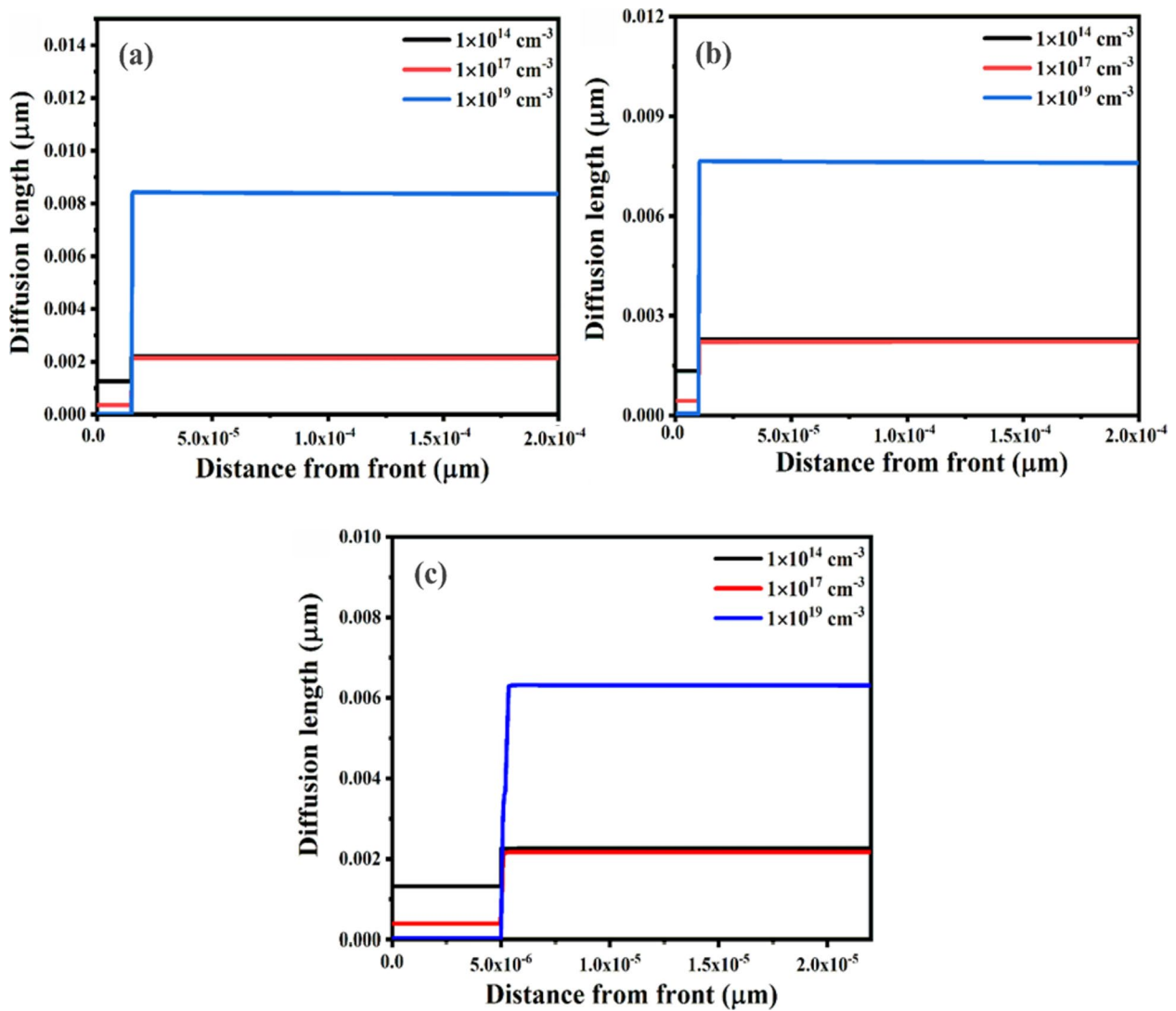

Fig. 7 Doping concentration dependent minority carrier diffusion length plots for three different configurations **a** *p*185, *n*15 μm **b** *p*190, *n*10 μm, and **c** *p*195, *n*5 μm
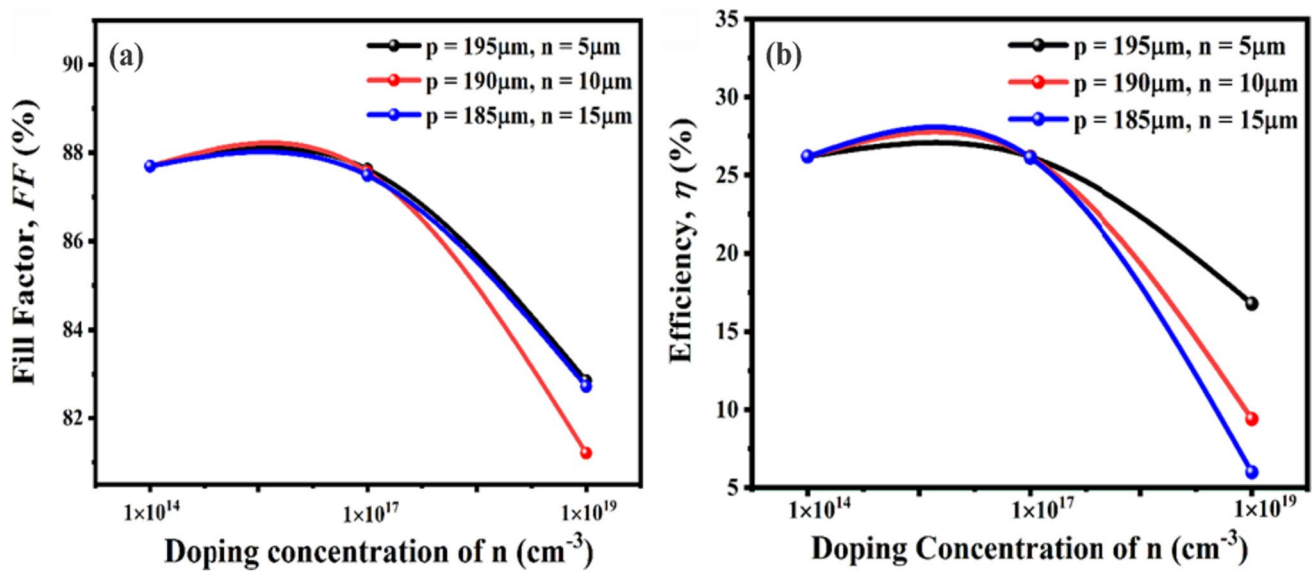
Fig. 8 **a** Fill factor versus doping concentration and **b** Efficiency versus doping concentration curve of the *n*-type wafer with different doping levels

Conclusion

We have demonstrated the model and successful optimization of a monocrystalline silicon solar cell on a nano-engineered surface-modified low-reflective Si substrate. We have experimentally obtained a highly stable nano-textured surface with an average reflectance of 0.652% useful for high light propagation. The work is focused on PC1D simulation software for different doping concentrations of the *n*-type layer that also involves the variation of the thickness of both layers (*p*-type and *n*-type) to increase photovoltaic efficiency. Our results suggest that *p*-type and *n*-type regions incorporating concentrations (low, medium, and/or high) offer a promising way to improve silicon solar cell structures' efficiency. Low and medium doping concentration levels (1×10^{14} and 1×10^{17} cm^{-3}, gradually) occurred with higher generation and recombination for charge carriers with adequate light trapping. Among them, low-level doping concentration (1×10^{14} cm^{-3}) gained the highest efficiency (26.19%) for all the photovoltaic cells with various p-type and n-type thicknesses. Diffusion length and photovoltaic parameters i.e., shunt resistance, series resistance, fill factor, and efficiency, have confirmed the effects of different doping concentrations enhancing the behavior of a junction of solar cells. It should be noted that semiconductor materials' expense is still a critical element in determining the practicality of constructing a solar device. Consequently, choosing materials with the right thickness and doping concentration is crucial to keeping costs down while increasing device efficiency. Finally, based on the accuracy, constancy, and predictability of PC1D, this article reveals the highest efficiency

for specified thickness (*n*-type and *p*-type) and doping region as a viable substitute in the investigation and upliftment status of producing crystalline Si solar cells. However, this is an ongoing research project and will be continued toward the process parameters optimization to fabricate of high-performing Si solar cells (lab-scale) in the near future.

Availability of data and materials The raw/processed data required to reproduce these findings cannot be shared at this time as the data also forms part of an ongoing study.

Declarations

Conflict of interests The authors declare that they have no known competing financial interests or personal relationships that could have appeared to influence the work reported in this paper.

References

1. M. Gul, Y. Kotak, T. Muneer, Review on recent trend of solar photovoltaic technology. Energy Explor. Exploit. **34**, 485–526 (2016). https://doi.org/10.1177/0144598716650552
2. H. Li, S. Guo, L. Cui, J. Yan, J. Liu, B. Wang, Review of renewable energy industry in Beijing: Development status, obstacles

and proposals. Renew. Sustain. Energy Rev. **43**, 711–725 (2015). https://doi.org/10.1016/j.rser.2014.11.074

3. J.-N. Kang, Y.-M. Wei, L.-C. Liu, R. Han, B.-Y. Yu, J.-W. Wang, Energy systems for climate change mitigation: A systematic review. Appl. Energy **263**, 114602 (2020). https://doi.org/10.1016/j.apenergy.2020.114602

4. N. Das, D. Chandrasekar, M. Nur-E-Alam, M.M.K. Khan, Light reflection loss reduction by nano-structured gratings for highly efficient next-generation gaas solar cells. Energies **13**, 4198 (2020). https://doi.org/10.3390/en13164198

5. T. Walker, M.E. Stuckelberger, T. Nietzold, N. Mohan-Kumar, C. Ossig, M. Kahnt, F. Wittwer, B. Lai, D. Salomon, E. Colegrove, M.I. Bertoni, The nanoscale distribution of copper and its influence on charge collection in CdTe solar cells. Nano Energy **91**, 106595 (2022). https://doi.org/10.1016/j.nanoen.2021.106595

6. S. Shafian, G. Eun Lee, H. Yu, J. Jeong, K. Kim, High-efficiency vivid color cigs solar cell employing nondestructive structural coloration. Sol. RRL. **6**, 2100965 (2022). https://doi.org/10.1002/solr.202100965

7. R. Anil Kumar, M.S. Suresh, J. Nagaraju, Measurement and comparison of AC parameters of silicon (BSR and BSFR) and gallium arsenide (GaAs/Ge) solar cells used in space applications. Sol. Energy Mater. Sol. Cells **60**, 155–166 (2000). https://doi.org/10.1016/S0927-0248(99)00080-X

8. M.K. Hossain, M.F. Pervez, M.N.H. Mia, S. Tayyaba, M.J. Uddin, R. Ahamed, R.A. Khan, M. Hoq, M.A. Khan, F. Ahmed, Annealing temperature effect on structural, morphological and optical parameters of mesoporous TiO2 film photoanode for dye-sensitized solar cell application. Mater. Sci. (2018). https://doi.org/10.1515/msp-2017-0082

9. M.K. Hossain, M.F. Pervez, M.J. Uddin, S. Tayyaba, M.N.H. Mia, M.S. Bashar, M.K.H. Jewel, M.A.S. Haque, M.A. Hakim, M.A. Khan, Influence of natural dye adsorption on the structural, morphological and optical properties of TiO 2 based photoanode of dye-sensitized solar cell. Mater. Sci. **36**, 93–101 (2017). https://doi.org/10.1515/msp-2017-0090

10. M.K. Basher, M.K. Hossain, M.A.R. Akand, Effect of surface texturization on minority carrier lifetime and photovoltaic performance of monocrystalline silicon solar cell. Optik (Stuttg). **176**, 93–101 (2019). https://doi.org/10.1016/j.ijleo.2018.09.042

11. M.K. Basher, M.K. Hossain, M.J. Uddin, M.A.R. Akand, K.M. Shorowordi, Effect of pyramidal texturization on the optical surface reflectance of monocrystalline photovoltaic silicon wafers. Optik (Stuttg). **172**, 801–811 (2018). https://doi.org/10.1016/j.ijleo.2018.07.116

12. M.K. Basher, M.K. Hossain, R. Afaz, S. Tayyaba, M.A.R. Akand, M.T. Rahman, N.M. Eman, Study and investigation of phosphorus doping time on emitter region for contact resistance optimization of monocrystalline silicon solar cell. Results Phys. **10**, 205–211 (2018). https://doi.org/10.1016/j.rinp.2018.05.038

13. S. Kalytchuk, S. Gupta, O. Zhovtiuk, A. Vaneski, S.V. Kershaw, H. Fu, Z. Fan, E.C.H. Kwok, C.-F. Wang, W.Y. Teoh, A.L. Rogach, Semiconductor nanocrystals as luminescent down-shifting layers to enhance the efficiency of thin-film CdTe/CdS and crystalline Si solar cells. J. Phys. Chem. C **118**, 16393–16400 (2014). https://doi.org/10.1021/jp410279z

14. J. Linghu, L. Shen, M. Yang, S. Xu, Y.P. Feng, Si 24: An efficient solar cell material. J. Phys. Chem. C **121**, 15574–15579 (2017). https://doi.org/10.1021/acs.jpcc.7b04032

15. G. Chen, I. Kashkoush, D. Nemeth, J. Rieker, A. Danel, Development of IPA-free Texturing Processes in Advanced Solar Cell Fabrication. In: Proc. 29th Eur. Photovolt. Sol. Energy Conf. Exhib, pp. 1096–1099, (2014)

16. S.C. Baker-Finch, K.R. McIntosh, Reflection distributions of textured monocrystalline silicon: Implications for silicon solar cells.

17. M.S. Kim, J.H. Lee, M.K. Kwak, Review: Surface texturing methods for solar cell efficiency enhancement. Int. J. Precis. Eng. Manuf. **21**, 1389–1398 (2020). https://doi.org/10.1007/s12541-020-00337-5

18. S.W. Glunz, High-efficiency crystalline silicon solar cells. Adv. Optoelectron. **2007**, 1–15 (2007). https://doi.org/10.1155/2007/97370

19. Y. Zhang, B. Wang, X. Li, Z. Gao, Y. Zhou, M. Li, D. Zhang, K. Tao, S. Jiang, H. Ge, S. Xiao, R. Jia, A novel additive for rapid and uniform texturing on high-efficiency monocrystalline silicon solar cells. Sol. Energy Mater. Sol. Cells **222**, 110947 (2021). https://doi.org/10.1016/j.solmat.2020.110947

20. Y. Jiang, X. Zhang, F. Wang, Y. Zhao, Optimization of a silicon wafer texturing process by modifying the texturing temperature for heterojunction solar cell applications. RSC Adv. **5**, 69629–69635 (2015). https://doi.org/10.1039/C5RA09739H

21. C.-Y. Huang, G.-C. Lin, Y.-J. Wu, T.-Y. Lin, Y.-J. Yang, Y.-F. Chen, Efficient light harvesting by well-aligned In_2O_3 nanopushpins as antireflection layer on si solar cells. J. Phys. Chem. C **115**, 13083–13087 (2011). https://doi.org/10.1021/jp201687k

22. T. Sakata, N. Ikeda, T. Koganezawa, D. Kajiya, K. Saitow, Performance of Si/PEDOT:PSS solar cell controlled by dipole moment of additives. J. Phys. Chem. C **123**, 20130–20135 (2019). https://doi.org/10.1021/acs.jpcc.9b05144

23. Y. Liu, M. Pomaska, W. Duan, D. Qiu, S. Li, A. Lambertz, A. Gad, U. Breuer, F. Finger, U. Rau, K. Ding, Phosphorus catalytic doping on intrinsic silicon thin films for the application in silicon heterojunction solar cells. ACS Appl. Mater. Interfaces **12**, 56615–56621 (2020). https://doi.org/10.1021/acsami.0c17416

24. A. Kolay, D. Maity, P. Ghosal, M. Deepa, Selenium Nanoparticle-decorated silicon nanowires with enhanced liquid-junction photoelectrochemical solar cell performance. J. Phys. Chem. C **123**, 8614–8622 (2019). https://doi.org/10.1021/acs.jpcc.9b00062

25. X.F. Gou, P. Wang, L.K. Jiang, S. Song, Y. Xu, Optimization of texturization on monocrystalline silicon solar cell. Adv. Mater. Res. **239–242**, 1322–1325 (2011). https://doi.org/10.4028/www.scientific.net/AMR.239-242.1322

26. Q. Fan, Z. Wang, Y. Cui, Optimal design of an antireflection coating structure for enhancing the energy-conversion efficiency of a silicon nanostructure solar cell. RSC Adv. **8**, 34793–34807 (2018). https://doi.org/10.1039/C8RA03730B

27. E. Manea, E. Budianu, M. Purica, D. Cristea, I. Cernica, R. Muller, V. Moagar Poladian, Optimization of front surface texturing processes for high-efficiency silicon solar cells. Sol. Energy Mater. Sol. Cells **87**, 423–431 (2005). https://doi.org/10.1016/j.solmat.2004.06.013

28. Z. Yang, J. Yan, W. Yang, Y. Zeng, J. Sun, X. Wang, X. Yang, J.C. Greer, J. Sheng, B. Yan, J. Ye, Back-contact structures for optoelectronic devices: Applications and perspectives. Nano Energy **78**, 105362 (2020). https://doi.org/10.1016/j.nanoen.2020.105362

29. G. Paternoster, *Silicon concentrator solar cells: fabrication, characterization and development of innovative designs* (University of Trento, 2013)

30. A. Mahmoud Al, B. Lahlouh, Silicon pyramid structure as a reflectivity reduction mechanism. J. Appl. Sci. **17**, 374–383 (2017). https://doi.org/10.3923/jas.2017.374.383

31. Q. He, W. Sheng, M. Zhang, G. Xu, P. Zhu, H. Zhang, Z. Yao, F. Gao, F. Liu, X. Liao, Y. Chen, Revealing morphology evolution in highly efficient bulk heterojunction and pseudo-planar heterojunction solar cells by additives treatment. Adv. Energy Mater. **11**, 2003390 (2021). https://doi.org/10.1002/aenm.202003390

32. P. Sundarapura, X.-M. Zhang, R. Yogai, K. Murakami, A. Fave, M. Ihara, Nanostructure of porous Si and anodic SiO_2 surface

Prog. Photovoltaics Res. Appl. (2012). https://doi.org/10.1002/pip.2186

passivation for improved efficiency porous si solar cells. Nanomaterials **11**, 459 (2021). https://doi.org/10.3390/nano11020459

33. A. Uzum, M. Kuriyama, H. Kanda, Y. Kimura, K. Tanimoto, H. Fukui, T. Izumi, T. Harada, S. Ito, Sprayed and spin-coated multilayer antireflection coating films for nonvacuum processed crystalline silicon solar cells. Int. J. Photoenergy **2017**, 1–5 (2017). https://doi.org/10.1155/2017/3436271

34. S. Iqbal, D. Su, H.L. Zhou, T. Zhang, Highly efficient and less time consuming additive free anisotropic etching of silicon wafers for photovoltaics. SILICON **12**, 773–778 (2020). https://doi.org/10.1007/s12633-019-00157-x

35. M.K. Basher, R. Mishan, S. Biswas, M.K. Hossain, M.A.R. Akand, M.A. Matin, Study and analysis the Cu nanoparticle assisted texturization forming low reflective silicon surface for solar cell application. AIP Adv. **9**, 075118 (2019). https://doi.org/10.1063/1.5109003

36. B. Hussain, A. Aslam, T. Khan, M. Creighton, B. Zohuri, Electron affinity and bandgap optimization of zinc oxide for improved performance of ZnO/Si heterojunction solar cell using PC1D simulations. Electronics **8**, 238 (2019). https://doi.org/10.3390/electronics8020238

37. G. Hashmi, A.R. Akand, M. Hoq, H. Rahman, Study of the enhancement of the efficiency of the monocrystalline silicon solar cell by optimizing effective parameters using PC1D simulation. SILICON **10**, 1653–1660 (2018). https://doi.org/10.1007/s12633-017-9649-3

38. S.-Y. Lien, D.-S. Wuu, Simulation and fabrication of heterojunction silicon solar cells from numerical computer and hot-wire CVD. Prog. Photovoltaics Res. Appl. **17**, 489–501 (2009). https://doi.org/10.1002/pip.900

39. P. Chauhan, S. Agarwal, V. Srivastava, M.K. Sadanand, R. Hossain, J. Pandey, P. Madan, D.K. Lohia, M.A. Dwivedi, Kesterite CZTS based thin film solar cell: Generation, recombination, and performance analysis. J. Phys. Chem. Solids (2023). https://doi.org/10.1016/j.jpcs.2023.111631

40. P. Chauhan, S. Agarwal, V. Srivastava, S. Maurya, M.K. Hossain, J. Madan, R.K. Yadav, P. Lohia, D.K. Dwivedi, A.A. Alothman, Impact on generation and recombination rate in Cu_2ZnSnS_4 (CZTS) solar cell for Ag_2S and In_2Se_3 buffer layers with $CuSbS_2$ back surface field layer. Prog. Photovoltaics Res. Appl. (2023). https://doi.org/10.1002/pip.3743

41. M.K. Hossain, G.F.I. Toki, A. Kuddus, M.H.K. Rubel, M.M. Hossain, H. Bencherif, M.F. Rahman, M.R. Islam, M. Mushtaq, An extensive study on multiple ETL and HTL layers to design and simulation of high-performance lead-free $CsSnCl_3$-based perovskite solar cells. Sci. Rep. **13**, 2521 (2023). https://doi.org/10.1038/s41598-023-28506-2

42. M.K. Hossain, M.H.K. Rubel, G.F.I. Toki, I. Alam, M.F. Rahman, H. Bencherif, Effect of various electron and hole transport layers on the performance of $CsPbI_3$-based perovskite solar cells: A numerical investigation in DFT, SCAPS-1D, and wxAMPS frameworks. ACS Omega **7**, 43210–43230 (2022). https://doi.org/10.1021/acsomega.2c05912

43. M.F. Rahman, M.J.A.A. Habib, M.H. Ali, M.H.K.K. Rubel, M.R. Islam, A.BMd. Ismail, M.K. Hossain, Design and numerical investigation of cadmium telluride (CdTe) and iron silicide ($FeSi_2$) based double absorber solar cells to enhance power conversion efficiency. AIP Adv. **12**, 105317 (2022). https://doi.org/10.1063/5.0108459

44. S.K. Biswas, M.S. Sumon, K. Sarker, M.F. Orthe, M.M. Ahmed, A numerical approach to analysis of an environment-friendly sn-based perovskite solar cell with SnO_2 buffer layer using SCAPS-1D. Adv. Mater. Sci. Eng. **2023**, 1–10 (2023). https://doi.org/10.1155/2023/4154962

45. M. Burgelman, P. Nollet, S. Degrave, Modeling polycrystalline semiconductor solar cells. Thin Solid Films **361–362**, 527–532 (2000). https://doi.org/10.1016/S0040-6090(99)00825-1

46. A. Cuevas, Y. Wan, D. Yan, C. Samundsett, T. Allen, X. Zhang, J. Cui, J. Bullock, Carrier population control and surface passivation in solar cells. Sol. Energy Mater. Sol. Cells **184**, 38–47 (2018). https://doi.org/10.1016/j.solmat.2018.04.026

47. P.P. Altermatt, F. Geelhaar, T. Trupke, X. Dai, A. Neisser, E. Daub, Injection dependence of spontaneous radiative recombination in crystalline silicon: Experimental verification and theoretical analysis. Appl. Phys. Lett. **88**, 1–4 (2006). https://doi.org/10.1063/1.2218041

48. J. Park, V.A. Dao, S. Kim, D.P. Pham, S. Kim, A.H.T. Le, J. Kang, J. Yi, High Efficiency Inorganic/Inorganic Amorphous Silicon/Heterojunction Silicon Tandem Solar Cells. Sci. Rep. **8**, 15386 (2018). https://doi.org/10.1038/s41598-018-33734-y

49. F.E. Cherif, H. Sammouda, Strategies for high performance perovskite/c-Si tandem solar cells: Effects of bandgap engineering, solar concentration and device temperature. Opt. Mater. (Amst.) **106**, 109935 (2020). https://doi.org/10.1016/j.optmat.2020.109935

50. C. Outes, E.F. Fernández, N. Seoane, F. Almonacid, A.J. García-Loureiro, Numerical optimisation and recombination effects on the vertical-tunnel-junction (VTJ) GaAs solar cell up to 10,000 suns. Sol. Energy **203**, 136–144 (2020). https://doi.org/10.1016/j.solener.2020.04.029

51. S. Kondratenko, O. Kozak, S. Rozouvan, Y.I. Mazur, Y. Maidaniuk, J. Wu, S. Wu, Z.M. Wang, S. Chan, D. Kim, H. Liu, G.J. Salamo, Carrier dynamics and recombination in silicon doped InAs/GaAs quantum dot solar cells with AlAs cap layers. Semicond. Sci. Technol. **35**, 115018 (2020). https://doi.org/10.1088/1361-6641/abb1c7

52. Y.-C. Wang, C.-W. Chen, T.-Y. Su, T.-Y. Yang, W.-W. Liu, F. Cheng, Z.M. Wang, Y.-L. Chueh, Design of suppressing optical and recombination losses in ultrathin $CuInGaSe_2$ solar cells by Voronoi nanocavity arrays. Nano Energy **78**, 105225 (2020). https://doi.org/10.1016/j.nanoen.2020.105225

53. S.M. Amir-Al Zumahi, N. Arobi, M. Mahbubur Rahman, M. Kamal Hossain, M. Ara Jahan Rozy, M. Bashar, A. Amri, H. Kabir, M. Abul Hossain, F. Ahmed, Understanding the optical behaviors and the power conversion efficiency of novel organic dye and nanostructured TiO_2 based integrated DSSCs. Sol. Energy **225**, 129–147 (2021). https://doi.org/10.1016/j.solener.2021.07.024

54. D.S.H. Chan, J.C.H. Phang, Analytical methods for the extraction of solar-cell single- and double-diode model parameters from I-V characteristics. IEEE Trans. Electron Devices **34**, 286–293 (1987). https://doi.org/10.1109/T-ED.1987.22920

55. M. Turek, Current and illumination dependent series resistance of solar cells. J. Appl. Phys. **115**, 144503 (2014). https://doi.org/10.1063/1.4871017

56. Z.Z. Bandić, P.M. Bridger, E.C. Piquette, T.C. McGill, Electron diffusion length and lifetime in p-type GaN. Appl. Phys. Lett. **73**, 3276–3278 (1998). https://doi.org/10.1063/1.122743

57. X. Cai, X. Zhou, Z. Liu, F. Jiang, Q. Yu, An in-depth analysis of the silicon solar cell key parameters' optimal magnitudes using PC1D simulations. Optik (Stuttg). **164**, 105–113 (2018). https://doi.org/10.1016/j.ijleo.2018.02.102

58. D.K. Shah, D. KC, M.S. Akhtar, C.Y. Kim, O.-B. Yang, Vertically arranged zinc oxide nanorods as antireflection layer for crystalline silicon solar cell: A simulation study of photovoltaic properties. Appl. Sci. **10**, 6062 (2020). https://doi.org/10.3390/app10176062

59. G.A. Medvedkin, Effect of diffusion length and surface recombination on the photopleochroism of anisotropic crystals. Semiconductors **34**, 517–520 (2000). https://doi.org/10.1134/1.1188018

60. H. Mehmood, T. Tauqeer, H. Nasser, S. Hussain, R. Turan, Effect of Hole-Selective Molybdenum Oxide Work Function and Silicon Wafer Resistivity on Dopant-Free Asymmetric Silicon Heterostructure Solar Cell. In: Proc. 2017 Int. Renew. Sustain. Energy Conf., IEEE, pp. 1–5, (2017). https://doi.org/10.1109/IRSEC.2017.8477335.

61. S. Dabbabi, T. Ben Nasr, N. Kamoun-Turki, Parameters optimization of CIGS solar cell using 2D physical modeling. Results Phys. **7**, 4020–4024 (2017). https://doi.org/10.1016/j.rinp.2017.06.057

62. T. Kraus, O. Höhn, H. Hauser, B. Bläsi, Optoelectronic simulation of GaAs solar cells with angularly selective filters. J. Appl. Phys. **115**, 053103 (2014). https://doi.org/10.1063/1.4863775

63. J.L. Gray, The Physics of the Solar Cell. In: Handbook Photovoltaic Science Engineering, Wiley, pp. 61–112, (2005). https://doi.org/10.1002/0470014008.ch3

64. M.A. Green, E.D. Dunlop, G. Siefer, M. Yoshita, N. Kopidakis, K. Bothe, X. Hao, Solar cell efficiency tables (Version 61). Prog. Photovoltaics Res. Appl. **31**, 3–16 (2023). https://doi.org/10.1002/pip.3646